High concentration of ultrafine particles in the Amazon free troposphere produced by organic new particle formation

Bin Zhao[a,1], Manish Shrivastava[a], Neil M. Donahue[b,c,d,e], Hamish Gordon[b,f], Meredith Schervish[b,c], John E. Shilling[a], Rahul A. Zaveri[a], Jian Wang[g], Meinrat O. Andreae[h,i,j], Chun Zhao[k,l], Brian Gaudet[a], Ying Liu[a], Jiwen Fan[a], and Jerome D. Fast[a,1]

[a]Atmospheric Sciences and Global Change Division, Pacific Northwest National Laboratory, Richland, WA 99352; [b]Center for Atmospheric Particle Studies, Carnegie Mellon University, Pittsburgh, PA 15213; [c]Department of Chemistry, Carnegie Mellon University, Pittsburgh, PA 15213; [d]Department of Engineering and Public Policy, Carnegie Mellon University, Pittsburgh, PA 15213; [e]Department of Chemical Engineering, Carnegie Mellon University, Pittsburgh, PA 15213; [f]School of Earth and Environment, University of Leeds, Leeds LS2 9JT, United Kingdom; [g]Center for Aerosol Science and Engineering, Department of Energy, Environmental and Chemical Engineering, Washington University in St. Louis, St. Louis, MO 63130; [h]Multiphase Chemistry Department, Max Planck Institute for Chemistry, Mainz 55128, Germany; [i]Scripps Institution of Oceanography, University of California San Diego, La Jolla, CA 92093; [j]Department of Geology and Geophysics, King Saud University, Riyadh 11451, Saudi Arabia; [k]School of Earth and Space Sciences, University of Science and Technology of China, 230026 Hefei, China; and [l]Chinese Academy of Sciences Center for Excellence in Comparative Planetology, University of Science and Technology of China, 230026 Hefei, China

Edited by Steven C. Wofsy, Harvard University, Cambridge, MA, and approved August 24, 2020 (received for review April 9, 2020)

The large concentrations of ultrafine particles consistently observed at high altitudes over the tropics represent one of the world's largest aerosol reservoirs, which may be providing a globally important source of cloud condensation nuclei. However, the sources and chemical processes contributing to the formation of these particles remain unclear. Here we investigate new particle formation (NPF) mechanisms in the Amazon free troposphere by integrating insights from laboratory measurements, chemical transport modeling, and field measurements. To account for organic NPF, we develop a comprehensive model representation of the temperature-dependent formation chemistry and thermodynamics of extremely low volatility organic compounds as well as their roles in NPF processes. We find that pure-organic NPF driven by natural biogenic emissions dominates in the uppermost troposphere above 13 km and accounts for 65 to 83% of the column total NPF rate under relatively pristine conditions, while ternary NPF involving organics and sulfuric acid dominates between 8 and 13 km. The large organic NPF rates at high altitudes mainly result from decreased volatility of organics and increased NPF efficiency at low temperatures, somewhat counterbalanced by a reduced chemical formation rate of extremely low volatility organic compounds. These findings imply a key role of naturally occurring organic NPF in high-altitude preindustrial environments and will help better quantify anthropogenic aerosol forcing from preindustrial times to the present day.

aerosol | new particle formation | extremely low volatility organic compounds | Amazon | troposphere

Atmospheric aerosols influence cloud properties and Earth's radiative balance by serving as cloud condensation nuclei (CCN), in addition to directly affecting solar radiation (1, 2). Changes in aerosols during the industrial era constitute one of the largest uncertainties in anthropogenic radiative forcing of the climate (1, 3). New particle formation (NPF) from condensable vapors is the largest source of atmospheric aerosols (4) and is thought to contribute about half of the global CCN (4–6). Extremely intense NPF activity has been observed in the tropical upper troposphere, correlated with low temperature and low preexisting aerosol surface area (7, 8). As a result, in situ observations have consistently shown large regions with very high aerosol concentrations—often orders of magnitude higher than those at lower altitudes or outside the tropics (7, 9, 10). This large reservoir of aerosols is of great significance for the climate system, because it may not only affect local anvil and cirrus cloud properties but also deliver a great amount of CCN to the lower troposphere as new particles grow to CCN size (larger than around 60 nm) both locally and in subsiding air (6, 7, 11, 12). At the same time it contributes to maintaining the stratospheric aerosol background (8, 13).

Despite the environmental importance of this large aerosol reservoir, the precursors and chemical processes contributing to its formation remain unclear. To date, no direct observational evidence has been presented because of the difficulty in measuring the chemical composition of newly formed particles in the upper troposphere (7, 10). Model simulations constrained by available in situ measurements are one approach to elucidate the NPF mechanisms. A recent study by Williamson et al. (7), however, showed that four mainstream global climate models did not

Significance

The high-altitude tropics constitute one of the world's largest aerosol reservoirs, which may significantly affect clouds, radiation, and hydrological cycle by delivering the seeds on which clouds form to lower altitudes and maintaining the stratospheric aerosol background. However, the formation mechanisms of these aerosols remain a scientific mystery. Through a systematic experiment-based model representation of organic chemistry and new particle formation (NPF) combined with constraints from field measurements, we demonstrate that the NPF driven by extremely low volatility organics formed from biogenic emissions plays a key role in producing the large number of aerosols observed in the high-altitude Amazon. This organic NPF mechanism likely also prevailed during preindustrial times and hence may modulate anthropogenic aerosol forcing above the preindustrial baseline.

Author contributions: B.Z., M. Shrivastava, N.M.D., and J.D.F. designed research; B.Z., M. Shrivastava, B.G., and J.D.F. performed research; N.M.D., H.G., M. Schervish, J.W., M.O.A., C.Z., and Y.L. contributed new reagents/analytic tools; B.Z., M. Shrivastava, N.M.D., J.E.S., R.A.Z., J.F., and J.D.F. analyzed data; and B.Z., M. Shrivastava, N.M.D., H.G., M. Schervish, J.E.S., R.A.Z., J.W., M.O.A., C.Z., B.G., Y.L., J.F., and J.D.F. wrote the paper.

The authors declare no competing interest.

This article is a PNAS Direct Submission.

[1]To whom correspondence may be addressed. Email: bin.zhao@pnnl.gov or Jerome.Fast@pnnl.gov.

This article contains supporting information online at https://www.pnas.org/lookup/suppl/doi:10.1073/pnas.2006716117/-/DCSupplemental.

First published September 28, 2020.

reproduce either the magnitude of tropical upper tropospheric NPF or the amount of CCN formed from the new particles.

A major challenge in NPF simulation is the complexity of organic-mediated NPF, which may play a large and even dominant role in NPF processes, especially under pristine or preindustrial conditions (14–16). Many laboratory and field studies (15, 17–19) have shown that organic NPF is triggered by a large variety of ultra- and extremely low volatility organic compounds (ULVOC and ELVOC, defined as organics with saturation vapor concentration C^* smaller than 3×10^{-9} μg/m^3 and 3×10^{-5} μg/m^3, respectively). These compounds are formed mainly through autoxidation and dimerization processes (15, 17, 20), which are fundamentally different from traditional oxidation reactions and have seldom been considered in chemical transport models (CTMs). Both the formation chemistry and volatility of compounds comprising ULVOC/ELVOC depend strongly on temperature (18, 21). A number of studies have simulated organic NPF in three-dimensional CTMs (4, 16, 22–25). However, they either assumed the nucleating organics to be a fixed fraction of all oxidation products (4, 22–25) or assumed that only a few individual species would nucleate (16). Those assumptions are inconsistent with the latest scientific understanding described above and may lead to substantial bias in simulated organic NPF rates, considering that the number, yield, and volatility of the organic compounds that contribute to NPF may vary by several orders of magnitude with temperature (18, 21, 26).

Here we present an investigation of the formation mechanisms driving the high aerosol concentrations in the Amazon free troposphere through a combination of regional chemical transport modeling and intensive field measurements. We incorporate in WRF-Chem (Weather Research and Forecasting model with Chemistry) (27) an experimentally constrained radical two-dimensional volatility basis set (2D-VBS) framework and seven different NPF processes. This framework attempts to comprehensively simulate the temperature-dependent formation chemistry (including autoxidation and dimerization) and volatility distribution of low-volatility organic compounds generated from monoterpenes and their role in NPF processes. The model developments bring simulated aerosol vertical profiles and size distributions into good agreement with in situ measurements and demonstrate a key role of organic-mediated NPF in producing the large upper-tropospheric aerosol reservoir above the Amazon rainforest. The Amazon is one of the few remaining places on Earth where atmosphere approaches preindustrial conditions at certain times (28–30). Understanding the aerosol sources and characteristics in such a preindustrial-like environment is important for quantifying anthropogenic aerosol radiative forcing resulting from differences between the present day and preindustrial times (31, 32).

Results

Simulated Particle Formation Pathways. Using the WRF-Chem model with our developments in the representation of ULVOC/ELVOC and NPF processes, we conduct simulations over a domain covering the central Amazon basin with 10-km grid spacing (Fig. 1) for a wet-season period (6 March to 15 March) and a dry-season period (10 September to 16 September) in 2014 (see detailed model configurations in *SI Appendix*, section 2). Fig. 2 *A* and *B* illustrates the aerosol number size distribution simulated by our best-case scenario (abbreviated to "inorg+org_2D-VBS"; see *SI Appendix*, Table S1 for a list of all scenarios). This scenario represents a comprehensive ensemble of inorganic and organic NPF pathways and uses the radical 2D-VBS to calculate the organics contributing to NPF. The model parameters of the radical 2D-VBS are constrained against laboratory experiments at atmospherically relevant conditions in this study to reasonably represent the chemical processes in the real atmosphere. To minimize the effect of human activity, we focus the analysis on a relatively clean area within the domain (red dashed rectangle in Fig. 1). This area was seldom affected by urban plumes during the simulation periods and was much less affected by biomass burning than other areas in the domain. Previous studies (7, 10) have shown that the high upper-tropospheric aerosol concentration is a common phenomenon regardless of whether there is urban pollution or biomass burning in the region below; our simulation results confirm this (*SI Appendix*, Fig. S1). The aerosol number concentrations increase sharply from the lower to upper troposphere over the relatively clean area during both wet and dry seasons (Fig. 2 *A* and *B*), consistent with existing observations in relatively clean conditions above the Amazon (10, 11). The size distribution in the uppermost troposphere (>13 km) is dominated by a nucleation mode with diameters smaller than about 12 nm. The distribution generally shifts to a larger size as height decreases, and an accumulation mode (55 to 400 nm) becomes prominent near the surface.

In our best-case simulation, over 95% of the aerosol concentration above 8 km originates from NPF within the modeling domain, although the percentage of contribution gradually decreases at lower altitudes (*SI Appendix*, Fig. S2). The NPF rates

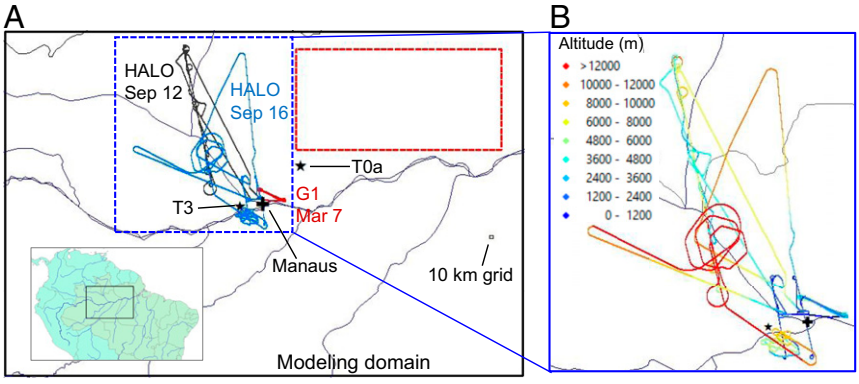

Fig. 1. Modeling domain and locations of measurements used in this study. (*A*) The WRF-Chem modeling domain with a 10-km grid spacing. (*Inset*) The location of the domain in South America. The red rectangle defines the part of the modeling domain used for most analysis in this study—a relatively clean area that was seldom affected by urban plumes and was much less affected by biomass burning than other areas in the domain during our simulation periods. The colored lines show flight tracks of the Gulfstream 1 (G-1) aircraft on 7 March 2014 as part of the GoAmazon (Observations and Modeling of the Green Ocean Amazon) campaign (58) and those of the HALO (German High Altitude and LOng range) aircraft on 12 and 16 September 2014 as part of the ACRIDICON-CHUVA campaign (59). These three flights primarily flew over relatively pristine regions. The black stars denote the T0a (ATTO) and T3 surface sites and the black cross denotes the location of Manaus, an isolated megacity in the central Amazon basin with about 2 million people. (*B*) Aircraft flight tracks colored by altitude.

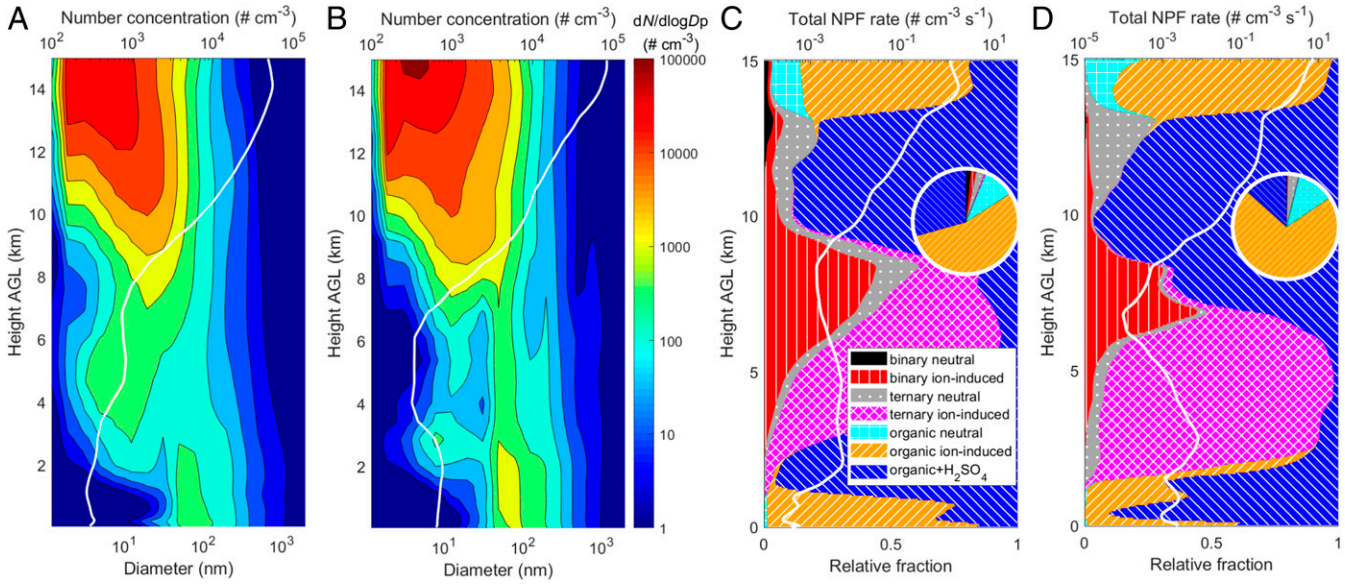

Fig. 2. Averaged aerosol number size distributions and NPF rates as a function of height above ground level (AGL). (*A* and *B*) Averaged aerosol number size distributions simulated by the comprehensive best-case ensemble of NPF processes over relatively clean areas (red dashed rectangle in Fig. 1) during the (*A*) wet season and (*B*) dry season periods. The white line is the total number concentration of aerosols larger than 3-nm diameter (N_3). The aerosol number concentration and size distribution are normalized to standard temperature and pressure (STP; 273.15 K and 101.325 kPa). Note that we extended the eight size bins (covering 39 nm to 10 μm) in the original WRF-Chem model to 20 size bins ranging from 1 nm to 10 μm. (*C* and *D*) Total NPF rate at a diameter of 1.7 nm ($J_{1.7}$, white line, on a log scale) and relative contribution of seven different NPF pathways (colored contours) averaged over relatively clean areas during the (*C*) wet season and (*D*) dry season periods. (*Insets*) The relative contribution to column total NPF rates. A similar figure for a larger height range (0 to 20 km) is provided in *SI Appendix*, Fig. S7.

at 1.7 nm diameter ($J_{1.7}$) in the uppermost troposphere (>13 km) are about three orders of magnitude larger than in the lower troposphere (Fig. 2 *C* and *D* and *SI Appendix*, Fig. S3), which explains the large number concentrations at high altitudes. Nevertheless, what processes contribute to the extremely high NPF rates remains unclear in the current literature. We show in Fig. 2 *C* and *D* the relative contribution of different NPF pathways as a function of height over the relatively clean area defined above. We consider four inorganic NPF pathways, including binary neutral and ion-induced NPF (involving H_2SO_4) and ternary neutral and ion-induced NPF (involving H_2SO_4 and NH_3), as well as three organic pathways, including pure-organic neutral and ion-induced NPF and ternary NPF of organics with H_2SO_4. In the troposphere above 13 km, pure-organic NPF dominates (>77%) during both seasons, of which ion-induced and neutral pathways account for 60 to 80% and 10 to 20%, respectively. As altitude decreases, NPF of organics with H_2SO_4 overtakes pure-organic NPF and becomes the main NPF pathway between 9 and 13 km during the wet season period and between 7 and 13 km during the dry season period (see the next paragraph for explanations). Considering that the NPF rates in the upper troposphere are orders of magnitude higher than those at lower altitudes, the above three pathways involving organics dominate the column total NPF rates in both seasons, with organic ion-induced, organic neutral, and organic+H_2SO_4 NPF contributing 55 to 71%, 10 to 12%, and 13 to 29%, respectively (Fig. 2 *C* and *D*, *Insets*). At lower altitudes (<9 km in wet season and <7 km in dry season), the dominant pathway is either organic+H_2SO_4 or ternary ion-induced NPF, depending on altitude, while binary ion-induced and organic ion-induced NPF also make considerable contributions at certain altitudes.

Obviously, the remarkably high NPF rates of the three organic-mediated pathways at high altitudes are key to producing the large upper tropospheric aerosol number concentrations in our simulation results. The pure-organic and organic+H_2SO_4 NPF is triggered by ULVOC and ELVOC with certain degrees of polarity (O:C >0.4) formed from monoterpenes, respectively, in our model (the potential effects of isoprene and sesquiterpenes are discussed later). Our systematic representation of the formation chemistry and thermodynamics of ULVOC/ELVOC allows an in-depth analysis of factors governing the NPF rates at high altitudes. First, as temperature decreases with increasing altitude, the distribution of monoterpene oxidation products shifts toward lower O:C and higher room-temperature volatility (i.e., volatility at 300 K) mainly because autoxidation is suppressed, as shown in previous experimental studies (17, 21) and captured by our radical 2D-VBS model. As a result, the fractions of ULVOC and ELVOC (referring only to those with O:C >0.4 hereafter) in all monoterpene oxidation products would gradually decrease, were the volatilities measured at 300 K (black lines in Fig. 3). Second, however, as temperature decreases, the volatility of organics decreases and thus many organic compounds with larger room-temperature volatility become ULVOC or ELVOC. Due to the competing effects of the above two factors, the fractions of ULVOC and ELVOC in all monoterpene oxidation products at ambient temperature first decrease slightly and then increase sharply with increasing altitude (blue lines in Fig. 3), indicating that the changes in chemistry and volatility successively play a leading role, with volatility more than winning out at high altitude. Further considering changes in the abundance of the total oxidation products, the mass mixing ratios of ULVOC and ELVOC exhibit a significant decrease from the surface to 7.5 km but then exhibit an even larger increase from 7.5 km to 15 km (red lines in Fig. 3). Third, the NPF rates of organics increase with decreasing temperature because low temperature helps to stabilize newly formed clusters (22, 33). Applying the temperature dependence of NPF rates (*Methods*) to ULVOC and ELVOC concentrations results in significantly larger organic NPF rates in the upper troposphere than at lower altitudes (Fig. 2 *C* and *D* and *SI Appendix*, Fig. S3). Note that

while the rates of both pure-organic and organic+H_2SO_4 NPF are much enhanced at high altitudes, the former dominates above 13 km and the latter dominates between 8 and 13 km (Fig. 2 *C* and *D*), because the former increases much more rapidly with height above 13 km. Laboratory experiments show that the rate of organic+H_2SO_4 NPF increases roughly linearly with organic concentration (34), while that of pure-organic NPF usually increases much quicker than linearly (15).

Constraint from In Situ Measurements. Comparison of our model results with in situ observations helps to constrain how different NPF pathways contribute to particle concentrations. To better examine the roles of inorganic and organic NPF mechanisms, we conduct several more simulations (*SI Appendix*, Table S1) in addition to our best-case scenario of "inorg+org_2D-VBS." We turn off all NPF processes in the "nonuc" case and include only inorganic NPF in the "inorg" case. In the "inorg+org_simple" case we include both inorganic and organic NPF; however, unlike the "inorg+org_2D-VBS" case that simulates organic chemistry with the radical 2D-VBS, "inorg+org_simple" adopts a simple assumption that the organics contributing to NPF are a fixed fraction of all monoterpene oxidation products, following the common practice of many previous studies (4, 14, 22–25). The specific fixed fractions we used are from Gordon et al. (4).

Fig. 4 compares the simulated vertical profiles of aerosol number concentration with measurements by the US Department of Energy Gulfstream 1 (G-1) and German High Altitude and LOng range (HALO) aircraft during three flights (7 March and 12 and 16 September; see details of the observational data in *SI Appendix*, section 3). Among all flights by the two aircraft, the ones we chose flew over different altitudes under relatively clean conditions for a sufficiently long time to permit a reasonable comparison. Therefore, they can be used to establish representative aerosol vertical profiles in the near-pristine environment over the Amazon. Without NPF ("nonuc"), simulated aerosol concentrations decrease remarkably with increasing altitude, contrary to the observed increasing trend; the model dramatically underestimates observed aerosol number in the free troposphere. With inorganic NPF included ("inorg"), the simulation results are noticeably improved, especially below 6 km. However, significant underestimation remains throughout most of the free troposphere, and only a small fraction of the aerosol number can be explained in the upper troposphere above 8 km. When organic NPF is simulated using the abovementioned simple method ("inorg+org_simple"), most new particles appear at low altitudes below 6 km, contradicting the observed vertical profile of aerosol number. Only when organic NPF is included and simulated more physically using the radical 2D-VBS ("inorg+org_2D-VBS") does the model reasonably reproduce the observed aerosol vertical profile. These results support our findings that the particle formation in the upper troposphere (>~8 km) may be dominated by organic-mediated NPF while both inorganic and organic NPF can play important roles in the free troposphere below 8 km.

We further compare simulated aerosol number size distributions with G-1 observations on 7 March at different altitudes (Fig. 5). Observations show that an Aitken mode (roughly 12- to 60-nm diameter) becomes more and more prominent with the increase in altitude and absolutely dominates the size distribution above 3,200 m. Without NPF ("nonuc"), the simulation can generally capture the accumulation mode (roughly 60 to 400 nm) but completely misses the Aitken mode above 1,900 m. The inclusion of inorganic NPF ("inorg") narrows the gap but still cannot reproduce the observed peaks of number density at most altitudes. Further incorporating organic NPF based on the radical 2D-VBS ("inorg+org_2D-VBS") bridges the remaining gap and results in a fairly good agreement with observations. A remaining bias is that the model underestimates small particles (<40-nm diameter) at the lowest altitude (Fig. 5*A*), probably because the 10-km grid spacing cannot fully capture the strong convective downdrafts that may rapidly transport small particles from the free troposphere into the boundary layer without significant growth (see more discussions in *SI Appendix*, section 4). In addition, the simulation results of our best-case scenario ("inorg+org_2D-VBS") are also generally consistent with observations of aerosol chemical

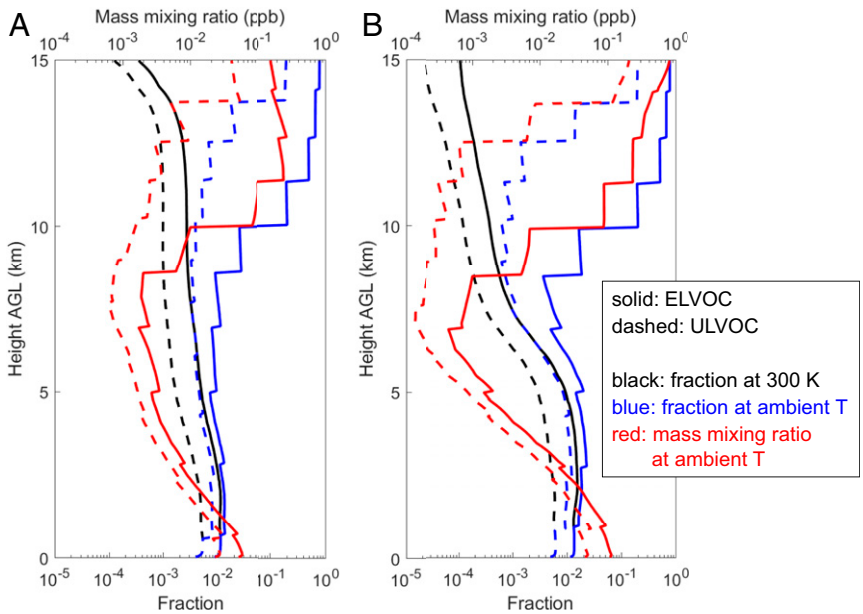

Fig. 3. Production and abundance of ULVOC and ELVOC. Averaged mass mixing ratio of ULVOC and ELVOC (red lines) and their fractions in all monoterpene oxidation products (black and blue lines) as a function of height during the (*A*) wet season and (*B*) dry season periods. Here ULVOC and ELVOC only refer to those with O:C >0.4 that drive organic-mediated NPF. The black lines are the fractions of ULVOC and ELVOC when ULVOC/ELVOC at all heights are defined based on their volatility at 300 K. The blue lines are the fractions of ULVOC and ELVOC in the temperature at which the air masses are located. The ULVOC/ELVOC mixing ratios and fractions are calculated by summing gas- and particle-phase compositions in the atmosphere, which approximately represents all ULVOC/ELVOC that have been formed from monoterpene oxidation. A similar figure for a larger height range (0 to 20 km) is provided in *SI Appendix*, Fig. S8.

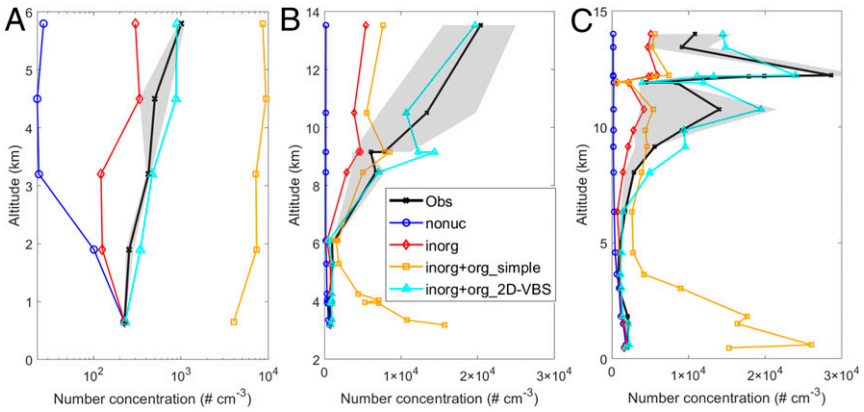

Fig. 4. Comparison of simulated vertical profile of aerosol number concentration with aircraft measurements. (*A*) Comparison with G-1 measurements on 7 March. Both simulations and observations are for particles with diameters larger than 3 nm (N_3). (*B* and *C*) Comparison with HALO measurements on (*B*) 12 September and (*C*) 16 September. Both simulations and observations are for particles larger than 10 nm (N_{10}) near the surface and 20 nm (N_{20}) above 13.8 km, with a smooth transition between the two heights. The difference in cut-off diameters between G-1 and HALO measurements is due to the difference in instruments. The lines are mean concentrations within each vertical bin while the shaded areas represent the 25th to 75th percentiles of the observations. All aerosol number concentrations are normalized to STP. The definitions of the model scenarios are provided in the section of *Constraint from In Situ Measurements* and in *SI Appendix*, Table S1. Details of the observational data are described in *SI Appendix, section 3*.

compositions and monoterpene concentrations which have established connections to NPF (*SI Appendix*, section 4). The constraints from the above observations further strengthen the robustness of our finding regarding the particle sources at high altitudes.

Sensitivity Analysis. Having shown the key role of organic NPF in upper-tropospheric aerosol formation, we acknowledge that organic NPF is still subject to uncertainties due to its high complexity, although we have built our model representation of organic chemistry and NPF upon ample experimental evidence and constrained our simulation results against field measurements. Here we identify a few key factors that may affect organic NPF in the upper troposphere and examine their potential impacts on our findings through sensitivity analyses. First, regarding the temperature dependence of autoxidation, we conduct two sensitivity experiments with higher ("high-barrier") and lower ("low-barrier") energy barriers for autoxidation than the base case (i.e., "inorg+org_2D-VBS"), resulting in stronger and weaker temperature dependence, respectively. Moreover, we design an experiment ("O:C-all") in which we assume that ULVOC and ELVOC with all O:C values (cf. just O:C >0.4 in the base case) contribute to NPF. The last two sensitivity experiments address the uncertainty in the temperature dependence of organic NPF rate by adopting stronger ("strong-T-dependence")

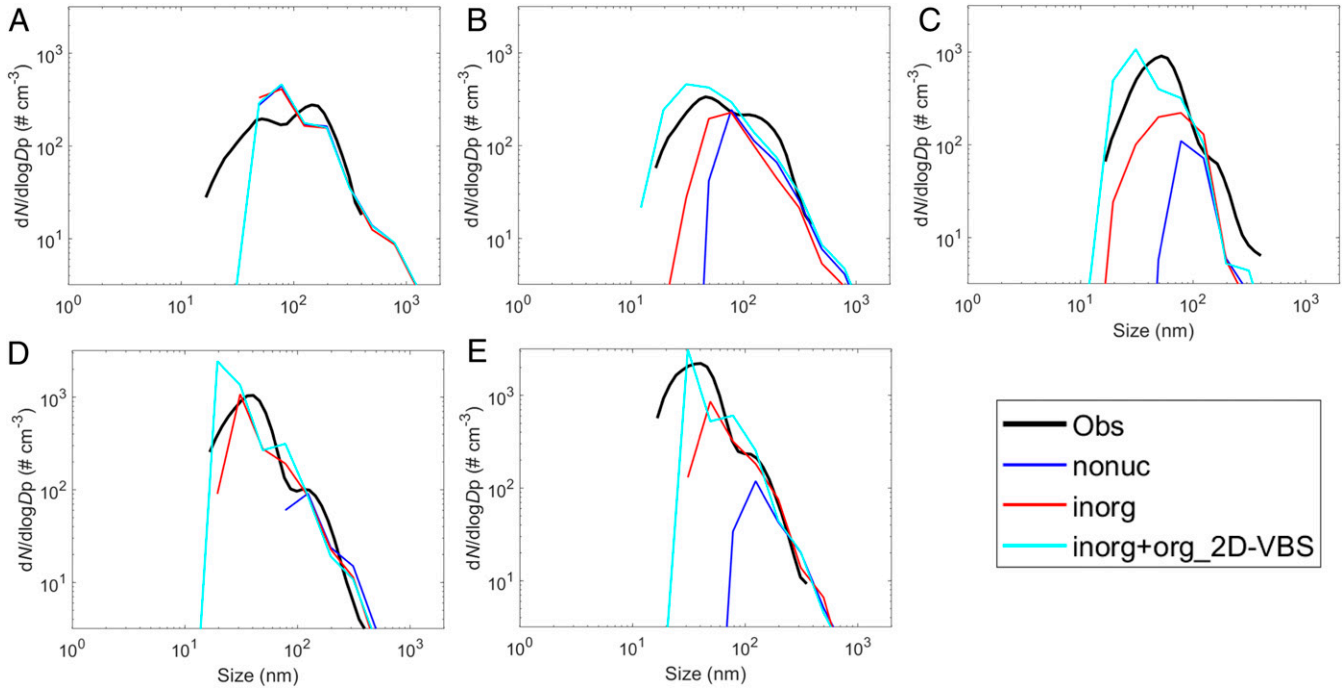

Fig. 5. Comparison of simulated aerosol number size distribution with G-1 measurements on 7 March at different altitudes: (*A*) 650 m, (*B*) 1,900 m, (*C*) 3,200 m, (*D*) 4,500 m, and (*E*) 5,800 m. All aerosol size distributions are normalized to STP. The definitions of the model scenarios are provided in the section of *Constraint from In Situ Measurements* and in *SI Appendix*, Table S1. Details of the observational data are described in *SI Appendix*, section 3.

and weaker ("weak-T-dependence") temperature dependence functions than the base case. More details of the sensitivity scenarios are provided in *SI Appendix*, section 5. While these simulations do induce some changes in simulated aerosol number concentration relative to the base case, they do not alter the general pattern of the vertical profile, which is consistent with the aircraft measurements (*SI Appendix*, Fig. S4). Also, these uncertainties do not change our main finding that the high aerosol number in the upper troposphere is mainly formed through pure-organic NPF (above 13 km) and organic+H_2SO_4 NPF (8–13 km; *SI Appendix*, Fig. S5). Finally, note that while we focused on monoterpenes as precursors to ULVOC and ELVOC that drive NPF previous studies have reported that sesquiterpenes might make a noticeable contribution to NPF despite their much smaller concentrations than monoterpenes (35). To the contrary, isoprene has been found to suppress secondary organic aerosol (SOA) and NPF from monoterpene oxidation products near surface (36–39), although the impact on NPF at high altitudes may be more complicated (see more in *SI Appendix*, section 8). While a quantitative modeling of these effects remains difficult due to limited experimental data, we speculate that the inclusion of these effects may affect only the magnitude but not the pattern of NPF rates.

Discussion

In this study, we demonstrated that organic NPF is a key formation pathway of the large numbers of small particles present at high altitudes over the Amazon. Many previous studies (6, 7, 10, 11) have shown that newly formed particles in the high-altitude tropics can be transported downward to lower altitudes and grow to larger sizes before, during, and after the subsidence, sustaining the particle number and CCN in the lower troposphere of relatively clean areas. Our analysis also reveals that the newly formed small particles are continuously transported downward throughout the troposphere (*SI Appendix*, Fig. S6 *A* and *B*). Through statistical analysis, we further show that this constant downward transport effectively enhances the aerosol number concentrations in relatively clean areas across a wide range of altitudes, ranging from the lower part of the upper troposphere to the bottom of the free troposphere (see details in *SI Appendix*, section 6). Regarding the gaseous species involved in particle growth, there is growing evidence that the condensation of organics probably dominates condensational growth over clean vegetated areas such as the Amazon (10, 40–42), both in the lower troposphere (10, 41) and upper troposphere (10, 40, 42, 43). However, further studies are needed to quantitatively evaluate how much ULVOC/ELVOC, other organics, and inorganic compounds contribute to particle growth at different altitudes.

A strength of this study is the systematic experiment-based characterization of the chemical properties and transformation of organics over a full range of volatility and temperature, as well as their linkage to NPF. Although the organic system is the most complicated and least understood aspect of aerosol formation, such a holistic characterization combined with constraint from in situ observations enables a detailed and robust source apportionment of particles at all heights throughout the troposphere. Since the tropical upper troposphere is a globally large source of atmospheric particles on a number basis (7, 10), a detailed attribution of the aerosol formation to specific NPF mechanisms helps improve the mechanistic understanding of the budgets of atmospheric particle number. Note, however, that it remains uncertain whether similar NPF mechanisms also play an important role in the tropical marine upper troposphere, where monoterpene concentrations are much lower (see more in *SI Appendix*, section 7). In addition, this study provides insight into the formation mechanisms and characteristics of aerosols in preindustrial times, which have been identified as one of the key uncertainties in estimates of anthropogenic aerosol forcing (31). We find that pure-organic NPF is a dominant particle source throughout the uppermost troposphere (above 13 km), accounting for over two-thirds of the column total NPF rates in relatively pristine conditions. This large particle source likely already existed in the preindustrial era, since it is primarily driven by natural biogenic sources. Meanwhile, our finding that the organic+H_2SO_4 NPF dominates particle formation between about 8 and 13 km suggests a close interaction between anthropogenic and biogenic emissions even for relatively pristine conditions. Therefore, our detailed analysis of the roles of different NPF mechanisms also improves the understanding of how anthropogenic activities perturb NPF, which helps shed light on anthropogenic aerosol forcing from preindustrial times to the present day. Finally, the large number of ultrafine aerosol particles (<50 nm) can impact clouds, precipitation, and lightning via secondary activation in deep convective cloud environments, especially in relatively pristine regions like the Amazon (44). Therefore, an improved understanding of the formation pathways of ultrafine particles will also help better predict the aerosol impact on precipitation and severe weather.

This study also has implications for the treatment of NPF processes in regional and global atmospheric models. We show that different NPF mechanisms dominate at different altitudes, similar to the findings of Dunne et al. (22) using a global model. This indicates that atmospheric models need to incorporate all NPF mechanisms considered in this study since they are competing for some of the same precursors. Also, atmospheric models need to adequately consider the temperature-dependent oxidation chemistry and volatility distribution of organics in order to reproduce the variation of ULVOC/ELVOC and the associated NPF as a function of altitude. The high level of complexity poses a critical challenge to atmospheric models, especially global models. In this study, we have condensed the organic species with the same room-temperature volatility but different O:C to improve computational efficiency; this simplification can also be adopted when incorporating the above processes in global models. In addition, compared with the 20 size bins used here, the modal representation of aerosol size distributions used in most global models imposes less computational burden. Also, the 17 volatility bins used in the current model can potentially be replaced by fewer bins with larger intervals (e.g., two-decade intervals instead of one-decade intervals in C*). In view of these considerations, the mechanisms proposed in this study have a great potential and feasibility to be incorporated in other regional and global models.

Methods

The Radical 2D-VBS Framework and Its Parameterization. We employ a radical 2D-VBS framework (18) and constrain its parameters against experimental data to simulate the chemical transformation and volatility distribution of monoterpene and its oxidation products (including ULVOC and ELVOC) over a full temperature range in the atmosphere. The 2D-VBS framework groups organic species into a space defined by volatility (C*) and oxygen-to-carbon ratio (O:C). In contrast to the traditional 2D-VBS, which tracks only stable molecules (45–47), the radical 2D-VBS explicitly represents peroxy radical (RO_2) chemistry and only distributes products into the 2D space after RO_2 termination into stable molecules (18). This feature enables an explicit modeling of autoxidation and dimerization processes, which are key formation pathways of ULVOC and ELVOC, as well as their competition with other reaction pathways. The chemical processes and key parameters within the radical 2D-VBS are described in *SI Appendix*, section 1.

In this study, we simulate a series of laboratory experiments with the radical 2D-VBS, compare modeled highly oxygenated organic molecule (HOM) yields and SOA concentrations with measurements, and optimize three key 2D-VBS parameters to achieve a good model–measurement agreement. The three key parameters are the fraction of first-generation peroxy radicals that can potentially autoxidize in all those formed via 1) the α-pinene + O_3 reaction (f_{O3}) and 2) the α-pinene + OH reaction (f_{OH}), and, finally, 3) the branching ratio between functionalization and fragmentation (*br*, meaning the fraction of fragmentation among the two reaction pathways). HOMs are organic compounds containing at least six oxygen atoms formed through autoxidation and subsequent termination processes (48). A significant fraction of HOMs comprises ULVOC and ELVOC (15, 18). We use available HOM measurements for α-pinene + O_3 (15, 49–51) and α-pinene + OH (15, 49, 50, 52) reactions to constrain the 2D-VBS parameters. We

use HOM yields instead of ULVOC/ELVOC yields because most experimental studies measured HOMs with widely used instruments such as chemical ionization mass spectrometers (CIMS) (15, 49, 50). For SOA concentrations, we employ laboratory experiments involving reactions of α-pinene with O_3 (53, 54) and OH (55), under both high-NO_x (54, 55) and low-NO_x (53–55) conditions. Based on these evaluations, we adopt $f_{O3} = 0.25$, $f_{OH} = 0.10$, and $br = (O:C)^{1/2}$, which results in an overall best agreement between modeled and measured HOM yields and SOA concentrations. *SI Appendix*, section 1 describes the details regarding the simulation of laboratory experiments, the comparison between modeled and experimental data, and the determination of parameters within the radical 2D-VBS framework. It should be noted that we constrained the 2D-VBS parameters mainly based on α-pinene oxidation experiments because most available HOM yield measurements are for α-pinene. Considering the larger HOM yields from α-pinene (representative of endocyclic monoterpene) than other monoterpenes found by Jokinen et al. (50), we apply an adjustment factor of 2/3 to the total HOM yields as endocyclic monoterpenes comprise nearly two-thirds of all monoterpene emissions over the Amazon (50).

Incorporation of the Radical 2D-VBS and NPF Parameterizations in WRF-Chem. We incorporate the radical 2D-VBS framework with experimentally constrained parameterization in WRF-Chem V4.1 and replace the current treatment of monoterpene gas-phase chemistry and equilibrium gas-particle partitioning in the model. We use 2D-VBS–simulated ULVOC and ELVOC with an O:C >0.4 to drive pure-organic and organic+H_2SO_4 NPF, respectively (18). We apply the O:C threshold because a certain degree of polarity favors the stabilization of newly formed clusters, especially in NPF involving ions or H_2SO_4. Also, nearly all clusters detected by CIMS during NPF processes have O:C >0.4, with few exceptions (15, 17, 21), supporting the above O:C threshold. However, since this O:C limit is still uncertain, we conduct a sensitivity simulation to examine its potential impact (*SI Appendix*, section 5).

We incorporate parameterizations of seven NPF pathways (discussed in the main text) in the MOSAIC (Model for Simulating Aerosol Interaction and Chemistry) aerosol module (56) of WRF-Chem and couple them with the 2D-VBS chemistry above. The parameterizations were developed and updated in several previous studies based on experiments in the CLOUD (Cosmics Leaving Outdoor Droplets) chamber (4, 15, 22, 34). The version we implement in WRF-Chem follows Gordon et al. (4), except for the following two updates. First, in view of the fact that the original parameterizations for pure-organic and organic+H_2SO_4 NPF used HOMs and total monoterpene oxidation products, respectively, as input variables, while we use ULVOC and ELVOC (with O:C larger than 0.4) instead, we adjust the original parameterizations linearly to suit the new input variables. The adjustment factors (3.6 and 33, respectively) are determined using the ratios between the original and new input variables under the environmental conditions where the original parameterizations were developed. Second, we apply a temperature dependence function to pure-organic and organic+H_2SO_4 NPF rates. Using quantum chemistry calculations, Dunne et al. (22) derived a temperature dependence function of $J_T = J_{278K}\exp(-(T-278)/10)$ for organic NPF, which results in a factor of 2.7 increase in NPF rate per 10 K temperature decrease. Yu et al. (33) obtained a stronger temperature dependence for organic NPF (about 1 order of magnitude increase per 10 K temperature decrease) based also on quantum chemistry calculations. These calculations were done for specific organic constituents. For ULVOC/ELVOC, however, the temperature dependence of the NPF rate is more complicated since they include different numbers of organic compounds at different temperatures. On the one hand, as temperature decreases, the compounds that were already ULVOC/ELVOC at high temperature will become even less volatile and hence accelerate the NPF rate, which can be captured by the quantum-chemistry-based functions. On the other hand, more compounds with higher room-temperature volatility will drift into the ULVOC/ELVOC range, buffering the temperature dependence of NPF rate to some extent, which is not accounted for by the quantum-chemistry-based functions. While it remains uncertain how strong the buffering effect is, our radical 2D-VBS shows that the mean C* of ULVOC decreases substantially from $10^{-9.2}$ μg/m^3 to $10^{-14.7}$ μg/m^3 as temperature decreases from 25 °C to −75 °C (roughly the range in the Amazon troposphere), indicating that the temperature dependence of NPF rate for ULVOC/ELVOC is substantial, though it is weaker than the calculation results of quantum chemistry. In view of the above, we apply a temperature dependence function of $J_T = J_{278K}\exp(-(T-278)/13.0)$ (a factor of 2.15 increase in NPF rate per 10 K temperature decrease), which is slightly weaker than the function of Dunne et al. (22) and much weaker than Yu et al. (33). We also perform two sensitivity simulations to examine the uncertainty in this temperature dependence (*SI Appendix*, section 5).

To account for the newly formed small particles and their initial growth, we extend the original eight size bins (covering 39 nm to 10 μm) in the MOSAIC aerosol module to 20 size bins (23) ranging from 1 nm to 10 μm. Since the 2D-VBS and the increased size bins will bring excessive computational burden, we add up the organic species with the same room-temperature volatility but different O:C for implementation in WRF-Chem. This equivalently condenses the 2D-VBS to a 1D-VBS involving 17 volatility bins with C* from 10^{-10} to 10^{6} μg/m^3 separated by 1 order of magnitude. Note, however, that all chemical equations incorporated in WRF-Chem are derived from the original radical 2D-VBS, so this simplification will just reduce the number of species advected in the model but will not bring bias to the simulation results. Finally, we modify the original MOSAIC aerosol scheme to account for the Kelvin effect (57).

We describe the configurations of the updated WRF-Chem model for application to the Amazon, including the vertical resolution, the physical and chemical schemes, the initial and boundary conditions, and the emission inventory, in *SI Appendix*, section 2.

Data Availability. The observational data used in this study are publicly available at https://www.arm.gov/research/campaigns/amf2014goamazon, http://lfa.if.usp.br/ftp/public/LFA_Processed_Data/T0a_ATTO, and https://halo-db.pa.op.dlr.de/mission/5. Other data supporting the findings of this study are available within the paper and *SI Appendix*. The raw output from the WRF-Chem model is available from the corresponding authors upon request.

ACKNOWLEDGMENTS. This research was funded by the US Department of Energy (DOE) Atmospheric System Research (ASR) program via the Integrated Cloud, Land-surface, and Aerosol System Study (ICLASS) Science Focus Area. The GoAmazon field campaign was supported by the Atmospheric Radiation Measurement (ARM) Climate Research Facility, a US DOE Office of Science User Facility, sponsored by the Office of Biological and Environmental Research. The Aerosol, Cloud, Precipitation, and Radiation Interactions and Dynamics of Convective Cloud Systems – Cloud Processes of the Main Precipitation Systems in Brazil: A Contribution to Cloud Resolving Modeling and to the Global Precipitation Measurement (ACRIDICON–CHUVA) campaign was supported by the Max Planck Society, the German Aerospace Center (DLR), FAPESP (São Paulo Research Founda-tion), and the German Science Foundation (Deutsche Forschungsgemeinschaft, DFG) within the DFG Priority Program (SPP 1294) "Atmospheric and Earth System Research with the Research Aircraft HALO." We thank the HALO science team for providing the ACRIDICON-CHUVA dataset, in particular D. Fütterer and B. Weinzierl, who collected the condensation particle counter data. For the operation of the ATTO site, we acknowledge the support by the German Federal Ministry of Education and Research (BMBF, contract 01LB1001A) and the Brazilian Ministério da Ciência, Tecnologia e Inovação (MCTI/FINEP, contract 01.11.01248.00) as well as the Amazon State University (UEA), the Fundação de Amparo à Pesquisa do Estado do Amazonas (FAPEAM), the Programa de Grande Escala da Biosfera-Atmosfera na Amazônia/Instituto Nacional de Pesquisas da Amazônia (LBA/INPA) and the Secretaria de Estado do Meio Ambiente e Desenvolvimento Sustentável/Centro Estadual de Unidades Climáticas/Reserva de Desenvolvimento Sustentável Uatumã (SDS/CEUC/RDS-Uatumã). We thank the ATTO science team for providing the SMPS dataset from that site. M. Shrivastava was also supported by the US DOE, Office of Science, Office of Biological and Environmental Research through the Early Career Research Program. N.M.D., M. Schervish, and H.G. were supported by the NASA ROSES project (Grant 80NSSC19K0949). J.W. acknowledges funding support from the DOE ASR program (Award DE-SC0020259). C.Z. was supported by the Fundamental Research Funds for the Central Universities of China and the National Natural Science Foundation of China (Grant 41775146). J.F. was supported by US DOE Early Career Research Program. Pacific Northwest National Laboratory (PNNL) is operated for DOE by the Battelle Memorial Institute under contract DE-A06-76RLO1830. Computational resources for the simulations were provided by the PNNL Institutional Computing (PIC) facility and the Environmental Molecular Sciences Laboratory (a DOE Office of Science User Facility sponsored by the Office of Biological and Environmental Research located at PNNL). We thank Dr. Jialei Zhu for insightful discussions.

1. IPCC, *Climate Change 2013: The Physical Science Basis. Contribution of Working Group I to the Fifth Assessment Report of the Intergovernmental Panel on Climate Change*, (Cambridge University Press, Cambridge, UK, 2013).
2. S. Twomey, Influence of pollution on shortwave albedo of clouds. *J. Atmos. Sci.* **34**, 1149–1152 (1977).
3. J. H. Seinfeld *et al*., Improving our fundamental understanding of the role of aerosol-cloud interactions in the climate system. *Proc. Natl. Acad. Sci. U.S.A.* **113**, 5781–5790 (2016).
4. H. Gordon *et al*., Causes and importance of new particle formation in the present-day and preindustrial atmospheres. *J. Geophys. Res. Atmos.* **122**, 8739–8760 (2017).

5. F. Yu, G. Luo, Simulation of particle size distribution with a global aerosol model: Contribution of nucleation to aerosol and CCN number concentrations. *Atmos. Chem. Phys.* **9**, 7691–7710 (2009).
6. J. Merikanto, D. V. Spracklen, G. W. Mann, S. J. Pickering, K. S. Carslaw, Impact of nucleation on global CCN. *Atmos. Chem. Phys.* **9**, 8601–8616 (2009).
7. C. J. Williamson *et al*., A large source of cloud condensation nuclei from new particle formation in the tropics. *Nature* **574**, 399–403 (2019).
8. R. Weigel *et al*., In situ observations of new particle formation in the tropical upper troposphere: The role of clouds and the nucleation mechanism. *Atmos. Chem. Phys.* **11**, 9983–10010 (2011).
9. A. D. Clarke *et al*., Nucleation in the equatorial free troposphere: Favorable environments during PEM-Tropics. *J. Geophys. Res. Atmos.* **104**, 5735–5744 (1999).
10. M. O. Andreae *et al*., Aerosol characteristics and particle production in the upper troposphere over the Amazon Basin. *Atmos. Chem. Phys.* **18**, 921–961 (2018).
11. J. Wang *et al*., Amazon boundary layer aerosol concentration sustained by vertical transport during rainfall. *Nature* **539**, 416–419 (2016).
12. B. Zhao *et al*., Impact of aerosols on ice crystal size. *Atmos. Chem. Phys.* **18**, 1065–1078 (2018).
13. C. A. Brock, P. Hamill, J. C. Wilson, H. H. Jonsson, K. R. Chan, Particle formation in the upper tropical troposphere: A source of nuclei for the stratospheric aerosol. *Science* **270**, 1650–1653 (1995).
14. H. Gordon *et al*., Reduced anthropogenic aerosol radiative forcing caused by biogenic new particle formation. *Proc. Natl. Acad. Sci. U.S.A.* **113**, 12053–12058 (2016).
15. J. Kirkby *et al*., Ion-induced nucleation of pure biogenic particles. *Nature* **533**, 521–526 (2016).
16. J. Zhu *et al*., Decrease in radiative forcing by organic aerosol nucleation, climate, and land use change. *Nat. Commun.* **10**, 423 (2019).
17. C. Frege *et al*., Influence of temperature on the molecular composition of ions and charged clusters during pure biogenic nucleation. *Atmos. Chem. Phys.* **18**, 65–79 (2018).
18. M. Schervish, N. M. Donahue, Peroxy radical chemistry and the volatility basis set. *Atmos. Chem. Phys.* **20**, 1183–1199 (2020).
19. F. Bianchi *et al*., New particle formation in the free troposphere: A question of chemistry and timing. *Science* **352**, 1109–1112 (2016).
20. Y. Zhao, J. A. Thornton, H. O. T. Pye, Quantitative constraints on autoxidation and dimer formation from direct probing of monoterpene-derived peroxy radical chemistry. *Proc. Natl. Acad. Sci. U.S.A.* **115**, 12142–12147 (2018).
21. Q. Ye *et al*., Molecular composition and volatility of nucleated particles from alpha-pinene oxidation between −50 degrees C and +25 degrees C. *Environ. Sci. Technol.* **53**, 12357–12365 (2019).
22. E. M. Dunne *et al*., Global atmospheric particle formation from CERN CLOUD measurements. *Science* **354**, 1119–1124 (2016).
23. A. Lupascu *et al*., Modeling particle nucleation and growth over northern California during the 2010 CARES campaign. *Atmos. Chem. Phys.* **15**, 12283–12313 (2015).
24. X. S. Chen *et al*., Improving new particle formation simulation by coupling a volatility-basis set (VBS) organic aerosol module in NAQPMS plus APM. *Atmos. Environ.* **204**, 1–11 (2019).
25. C. E. Scott *et al*., The direct and indirect radiative effects of biogenic secondary organic aerosol. *Atmos. Chem. Phys.* **14**, 447–470 (2014).
26. M. Simon *et al*., Molecular understanding of new-particle formation from alpha-pinene between −50 °C and 25 °C. *Atmos. Chem. Phys. Discuss.*, 10.5194/acp-2019-1058 (2020).
27. G. A. Grell *et al*., Fully coupled "online" chemistry within the WRF model. *Atmos. Environ.* **39**, 6957–6975 (2005).
28. M. Shrivastava *et al*., Urban pollution greatly enhances formation of natural aerosols over the Amazon rainforest. *Nat. Commun.* **10**, 1046 (2019).
29. U. Pöschl *et al*., Rainforest aerosols as biogenic nuclei of clouds and precipitation in the Amazon. *Science* **329**, 1513–1516 (2010).
30. M. L. Pohlker *et al*., Long-term observations of cloud condensation nuclei over the Amazon rain forest - Part 2: Variability and characteristics of biomass burning, long-range transport, and pristine rain forest aerosols. *Atmos. Chem. Phys.* **18**, 10289–10331 (2018).
31. K. S. Carslaw *et al*., Large contribution of natural aerosols to uncertainty in indirect forcing. *Nature* **503**, 67–71 (2013).
32. K. S. Carslaw *et al*., Aerosols in the pre-industrial atmosphere. *Curr. Clim. Change Rep.* **3**, 1–15 (2017).
33. F. Q. Yu, G. Luo, A. B. Nadykto, J. Herb, Impact of temperature dependence on the possible contribution of organics to new particle formation in the atmosphere. *Atmos. Chem. Phys.* **17**, 4997–5005 (2017).
34. F. Riccobono *et al*., Oxidation products of biogenic emissions contribute to nucleation of atmospheric particles. *Science* **344**, 717–721 (2014).
35. B. Bonn, G. K. Moortgat, Sesquiterpene ozonolysis: Origin of atmospheric new particle formation from biogenic hydrocarbons. *Geophys. Res. Lett.* **30**, 1585 (2003).
36. G. McFiggans *et al*., Secondary organic aerosol reduced by mixture of atmospheric vapours. *Nature* **565**, 587–593 (2019).
37. A. Kiendler-Scharr *et al*., New particle formation in forests inhibited by isoprene emissions. *Nature* **461**, 381–384 (2009).
38. S. H. Lee *et al*., Isoprene suppression of new particle formation: Potential mechanisms and implications. *J. Geophys. Res. Atmos.* **121**, 14621–14635 (2016).
39. M. Heinritzi, L. Dada, M. Simon, D. Stolzenburg, A. C. Wagner, Molecular understanding of the suppression of new-particle formation by isoprene. *Atmos. Chem. Phys. Discuss.*, 10.5194/acp-2020-5151 (2020).
40. A. M. L. Ekman *et al*., Do organics contribute to small particle formation in the Amazonian upper troposphere? *Geophys. Res. Lett.* **35**, L17810 (2008).
41. I. Riipinen *et al*., Organic condensation: A vital link connecting aerosol formation to cloud condensation nuclei (CCN) concentrations. *Atmos. Chem. Phys.* **11**, 3865–3878 (2011).
42. B. N. Murphy, J. Julin, I. Riipinen, A. M. L. Ekman, Organic aerosol processing in tropical deep convective clouds: Development of a new model (CRM-ORG) and implications for sources of particle number. *J. Geophys. Res. Atmos.* **120**, 10441–10464 (2015).
43. C. Schulz *et al*., Aircraft-based observations of isoprene-epoxydiol-derived secondary organic aerosol (IEPOX-SOA) in the tropical upper troposphere over the Amazon region. *Atmos. Chem. Phys.* **18**, 14979–15001 (2018).
44. J. Fan *et al*., Substantial convection and precipitation enhancements by ultrafine aerosol particles. *Science* **359**, 411–418 (2018).
45. N. M. Donahue, S. A. Epstein, S. N. Pandis, A. L. Robinson, A two-dimensional volatility basis set: 1. Organic-aerosol mixing thermodynamics. *Atmos. Chem. Phys.* **11**, 3303–3318 (2011).
46. N. M. Donahue, J. H. Kroll, S. N. Pandis, A. L. Robinson, A two-dimensional volatility basis set - Part 2: Diagnostics of organic-aerosol evolution. *Atmos. Chem. Phys.* **12**, 615–634 (2012).
47. B. Zhao *et al*., Quantifying the effect of organic aerosol aging and intermediate-volatility emissions on regional-scale aerosol pollution in China. *Sci. Rep.* **6**, 28815 (2016).
48. F. Bianchi *et al*., Highly oxygenated organic molecules (HOM) from gas-phase autoxidation involving peroxy radicals: A key contributor to atmospheric aerosol. *Chem. Rev.* **119**, 3472–3509 (2019).
49. M. Ehn *et al*., A large source of low-volatility secondary organic aerosol. *Nature* **506**, 476–479 (2014).
50. T. Jokinen *et al*., Production of extremely low volatile organic compounds from biogenic emissions: Measured yields and atmospheric implications. *Proc. Natl. Acad. Sci. U.S.A.* **112**, 7123–7128 (2015).
51. N. Sarnela *et al*., Measurement-model comparison of stabilized Criegee intermediate and highly oxygenated molecule production in the CLOUD chamber. *Atmos. Chem. Phys.* **18**, 2363–2380 (2018).
52. T. Berndt *et al*., Hydroxyl radical-induced formation of highly oxidized organic compounds. *Nat. Commun.* **7**, 13677 (2016).
53. J. E. Shilling *et al*., Particle mass yield in secondary organic aerosol formed by the dark ozonolysis of alpha-pinene. *Atmos. Chem. Phys.* **8**, 2073–2088 (2008).
54. A. A. Presto, N. M. Donahue, Investigation of alpha-pinene + ozone secondary organic aerosol formation at low total aerosol mass. *Environ. Sci. Technol.* **40**, 3536–3543 (2006).
55. N. L. Ng *et al*., Effect of NOx level on secondary organic aerosol (SOA) formation from the photooxidation of terpenes. *Atmos. Chem. Phys.* **7**, 5159–5174 (2007).
56. R. A. Zaveri, R. C. Easter, J. D. Fast, L. K. Peters, Model for simulating aerosol interactions and chemistry (MOSAIC). *J. Geophys. Res. Atmos.* **113**, D13204 (2008).
57. J. Tröstl *et al*., The role of low-volatility organic compounds in initial particle growth in the atmosphere. *Nature* **533**, 527–531 (2016).
58. S. T. Martin *et al*., The Green Ocean Amazon experiment (GoAmazon2014/5) observes pollution affecting gases, aerosols, clouds, and rainfall over the rain forest. *Bull. Am. Meteorol. Soc.* **98**, 981–997 (2017).
59. M. Wendisch *et al*., ACRIDICON-CHUVA campaign: Studying tropical deep convective clouds and precipitation over Amazonia using the new German research aircraft HALO. *Bull. Am. Meteorol. Soc.* **97**, 1885–1908 (2016).